Synthesis, characterization and structural study of new nickel(II) and mercury (II) complexes with imidazole oxime ligand

Mehdi Bouchouit, Hadjer Belahlou, Mounia Guergouri, Rafik Bensegueni, Sofiane Bouacida, El-Eulmi Bendeif, Karim Bouchouit, Abdelmalek Bouraiou

Synthesis, characterization and structural study of new Nickel(II) and Mercury (II) complexes with imidazole oxime ligand

Mehdi BOUCHOUIT,[a] Hadjer BELAHLOU,[a] Mounia GUERGOURI,[b] Rafik BENSEGUENI,[b,c] Sofiane BOUACIDA,[a,d] El-Eulmi BENDEIF,[e] Karim BOUCHOUIT,[f] Abdelmalek BOURAIOU[a*]

[a] Unité de Recherche de Chimie de l'Environnement et Moléculaire Structurale, Université des frères Mentouri, Constantine 25000, Algérie.
[b] Laboratoire de Chimie des Matériaux Constantine, Université des frères Mentouri-Constantine 1, 25000 Constantine, Algérie.
[c] Université Mohamed Cherif Messaadia, Souk Ahras, Algérie.
[d] Département Sciences de la Matière, Université Oum El Bouaghi, 04000 Oum El Bouaghi, Algérie.
[e] Université de Lorraine, CNRS, CRM2, Nancy, France.
[f] Laboratoire de Didactique des Sciences Physiques, Chimiques et Applications. Ecole Normal Supérieure de Constantine, Ville Universitaire, Constantine, Algérie.

[*]Corresponding Author. (A. Bouraiou) bouraiou.abdelmalek@umc.edu.dz, Tel: (+213 551 599 889)

Abstract:

In this work, we reported the experimental study of two new complexes named bis[chloro(1-methyl-1*H*-imidazole-2-carbaldehyde oxime) Nickel(II) $\{Ni(L)_2Cl_2\}$ (I) and Di-μ-chloro-bis[chloro(1-methyl-1*H*-imidazole-2-carbaldehyde oxime) mercury(II) $\{Hg_2(L)_2Cl_4\}$, DMF (II) based on (1-methylimidazole-2-aldoxime, L). The synthesis, crystallization, and characterization were detailed. Complex I display a hexa-coordinated compound with a distorted octahedral geometry. The Ni^{II} ion is coordinated to two ligands in bidentate mode through nitrogen atoms. Complex II has one unique Hg^{II} atom and forms a dimeric complex that contains two Hg^{II} atoms related by a crystallographic inversion centre. In this complex, the oxime ligand is ligated to the metal ion in a monodentate fashion through the nitrogen atoms. On the basis of bond distances, this complex exhibits a distorted tetrahedral geometry around each mercury centre metal. The complexes are analyzed using single-crystal diffraction, FT-IR, NMR, and UV-visible. Cyclic voltammetry was also used to understand the electrochemical behaviour of the ligand and both complexes. Furthermore, we have performed DFT calculations to get more about the spectral electronic transitions' nature, reactivity, and electronic structure of the ligand and complexes.

Keywords: Imidazole oxime; Complex; Single crystal; Cyclic voltammetry, DFT analysis.

1. Introduction

Transition metal ions are fundamental components of coordination complexes. Using ligands with several donor atoms is very beneficial since their metal complexes often lead to materials with beneficial physical properties and biological significance and can be exploited in diverse domains [1-2].

Oxime entities are widely recognized as versatile ligands, and their complexes with various transition metals have been studied since the beginning of the 20th century. The interest in oxime-containing coordination compounds is increasing due to their biological implications. The realization of their function and the metabolism mechanism in biological systems are connected with chelation by metal ions. Furthermore, oxime species play great importance in analytical chemistry and have been used extensively for detecting and separating transition metals [3-4].

In general, the reaction of oxime function with metal salts led to four coordination modes which confirm that the chemistry of metal-bonded oximes should be rich (Figure 1). The oxime ligand is potentially ambidentate and can coordinate with metal ions through nitrogen and/or oxygen atom(s), leading to mononuclear, dinuclear and trinuclear metal complexes [5].

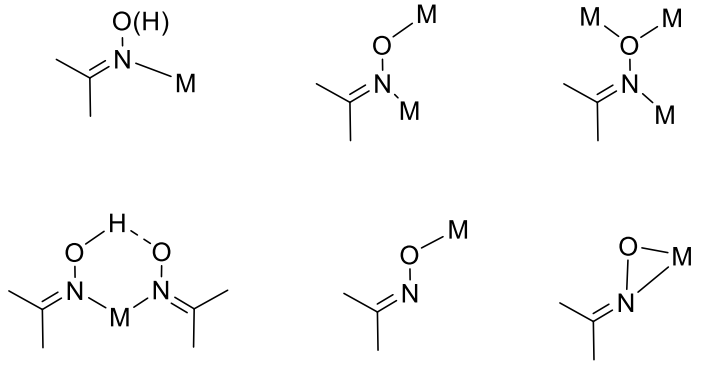

Fig. 1. The crystallographically established coordination modes of oxime and oximato groups.

Several recent papers have presented various topics, including synthetic pathways leading to oxime complexes and structural and different coordination modes (Figure 2). The binding mode of the oxime function depends not only on the coordinative ability of the oxime group but also on the presence of atom donors in the same molecule [6-9]. For example, imidazole oximes present several donor atoms in their structures. They are also very appealing ligands for synthesizing coordination compounds. The chelating behaviour of imidazole oxime and the different options for coordination are well established [9].

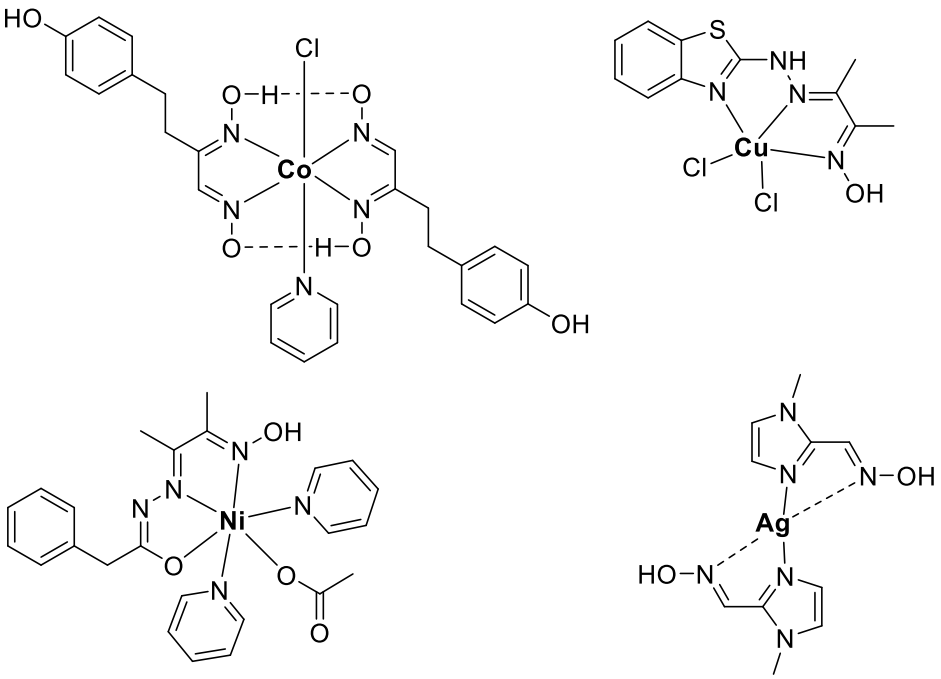

Fig. 2. Some previously reported oxime complexes [6-9].

In continuation of interest in the synthesis and characterization of coordination compounds, we report in the present work, the synthesis and structural characterization of nickel (II) and mercury (II) complexes containing 1-methyl-1*H*-imidazole-2-carbaldehyde oxime as a ligand. The electronic structure of the ligand and complexes are further studied using the DFT method, and several computational parameters such as E_{HOMO}, E_{LUMO}, ΔE, χ, η, σ and ΔN are calculated. The ligand and the two studied complexes were also characterized by cyclic voltammetry.

2. Experimental section

2.1. Materials and instrumentation

All the reagents and solvents were purchased from Aldrich, Acros Organics, and Merck and used without further purification. The melting point was determined using a Büchi M-565 Automatic Melting Point Apparatus. The NMR spectra of Ligand and complex II were recorded on a Bruker Avance 250 MHz mixture of $CDCl_3$ and DMSO-d^6. The UV spectra were recorded on an Optizen 1220 UV/VIS Spectrophotometer and FT-IR spectra were recorded on a Thermo Scientific Nicolet iS50 FTIR spectrophotometer. Single crystals of complexes I and II were grown by crystallizing the crude products in DMF. Crystallographic data for both structures were collected on a Bruker APEX II diffractometer equipped with an Apex II CCD detector using Mo-K_α radiation (microfocus sealed tube with a graphite monochromator). The crystal was coated with Paratone oil and mounted on loops for data

collection. The reported structure was solved by direct methods with SIR2002 [10] to locate all the non-H atoms, which were refined anisotropically with SHELXL97 [11] using full-matrix least-squares on the F2 procedure from within the WinGX [12] suite of software used to prepare material for publication. All absorption corrections were performed with the SADABS program [13]. All non-hydrogen atoms were refined anisotropically. Hydrogen atoms were placed in idealized geometrical positions and refined with *U*iso tied to the parent atom with the riding model. A Voltalab PGZ 301 was used in our experiments. The electrochemical study was carried out by cyclic voltammetry (CV) and performed using a three-electrode cell containing a glassy carbon disk (GCE) as the working electrode, a platinum wire as an auxiliary electrode, and a KCl-saturated calomel electrode (SCE). A 0.1 M solution of tetrabutylammonium tetrafluoroborate (Bu_4NBF_4) in dimethylsulfoxide was used as a supporting electrolyte. Before electrochemical measurements, all solutions were deaerated by argon bubbles for about 10 minutes.

2.2. Preparation of ligand L, complex I and complex II

2.2.1. Synthesis of -1-methyl-1H-imidazole-2-carbaldehyde oxime (L)

1-methyl-1*H*-imidazole-2-carbaldehyde oxime (L) has been synthesized following established methods. Spectroscopic results and physical properties agree with literature reports [14]. UV–Vis (DMF, λ_{max}/nm): 275; IR (cm^{-1}): 3120, 2990, 2920, 1670, 1630, 1520, 1470, 1420, 1280, 1150, 1080, 974, 936, 889, 837, 727, 687; ^{1}H NMR (250.13 MHz) δ (ppm): 11.46 (s_L, 1H), 8.08 (s, 1H), 6.96 (s, 2H), 3.81 (s, 3H)**;** ^{13}C NMR (62.9 MHz) δ (ppm): 141.1, 140.2, 128.0, 123.7, 34.9.

2.3.2. Synthesis of complexes

2.3.1. Preparation of {Ni(L)$_2$Cl$_2$} (I)

A mixture of a mixture of 1-methyl-1*H*-imidazole-2-carbaldehyde oxime (L) (2.0 mmol; 250.2 mg) and $NiCl_2$ (1.0 mmol; 129.6 mg) was dissolved in 10 ml of EtOH. The mixture was stirred for 18 hours. Solid were collected by filtration and dried in vacuo. Green powder; Yield 60 %; m.p. 229–230°C; UV–Vis (DMF, λ_{max}/nm): 278, 497, 634; IR (cm^{-1}): 2983, 1655, 1531, 1477, 1234, 1089, 926, 885, 628. Green crystals of I were obtained from dimethylformamide solution.

2.3.2. Preparation of {Hg$_2$(L)$_2$Cl$_4$}, DMF (II)

Complex II was obtained by a similar method as described for I**.** A mixture of 1-methyl-1H-imidazole-2-carbaldehyde oxime (L) (1.0 mmol; 125.1 mg) and $HgCl_2$ (1.0 mmol; 271.5 mg)

was dissolved in 10 ml of EtOH. The mixture was stirred for 18 hours. The obtained solid were collected by filtration and dried in vacuo. White powder; Yield 65 %; m.p. 180–183°C; UV–Vis (DMF, λ_{max}/nm): 278, 641; IR (cm^{-1}): 3404, 3006, 2962, 2360, 1655, 1549, 1491, 1429, 1373, 1291, 1274, 994, 968, 673; ^{1}H NMR (250.13 MHz) δ (ppm): 11.95 (sL, 1H), 8.33 (s, 1H), 7.15 (d, J=4.6Hz, 2H), 3.82 (s, 3H); ^{13}C NMR (62.9 MHz) δ (ppm): 140.1, 137.2, 126.8, 123.9, 34.7. White crystals of II were obtained from dimethylformamide solution.

3. Results and discussion

3.1. Chemistry and spectroscopic characterization

Following the established methods, we have prepared the oxime ligand, and the spectroscopic results and physical properties are in good agreement with the literature reports [14]. Complex I was obtained with a 60% yield from the reaction of one equivalent of $NiCl_2$ and two equivalents of the ligand L in ethanol. The reaction of equimolar amounts of $HgCl_2$ and the ligand L gave the corresponding complexes II with a 65% of yield (Scheme 1). The ligand and their metal complexes are stable at room temperature, are non-hygroscopic, soluble partially in methanol and ethanol and easily soluble in dimethylformamide.

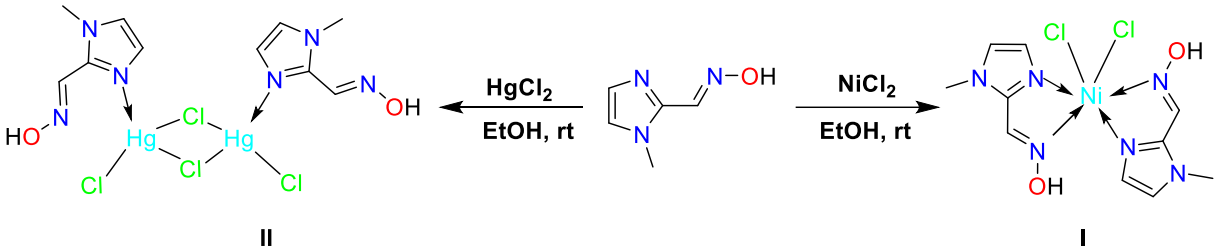

Scheme 1. Synthesis of complexes I and II**.**

Both complexes were characterized by spectroscopic methods, and their structures were confirmed by X–ray crystal structure analysis. The ^{1}H NMR spectra of the ligand (L) shows two signals at δ = 11.46 and δ = 8.08 ppm, which are assigned to NOH and HC=N protons, respectively (Scheme 1). The signal at δ = 6.96 ppm is assigned to two imidazole protons ring. Also, the signal at 3.81 ppm corresponds to protons of the methyl group. Complex II has similar spectra. Signals observed around 11.95 and 8.33 ppm are assigned to the NOH and HC=N protons. A signal at 7.15 ppm corresponds to imidazole protons. The signal at 3.82 ppm is due to protons of the methyl group. The ^{13}C NMR spectrum of the free ligand (L) shows a signal at 141.1 ppm, which may be assigned to azomethine carbon. While the resonance signals observed in the region 140.2–123.7 ppm were assigned to carbon atoms of the imidazole ring. In complex II, two aromatic signals have undergone a downfield shift and

appeared at 137.2 and 126.8 ppm from their expected positions, suggesting the involvement of nitrogen of the imidazole ring in coordination.

On the other hand, several studies have been made on the infrared spectra of oximes, and most of them have dealt with OH and C=N stretching vibration [15,16]. The simple Ligand (L) spectra exhibit an OH band at 3120 cm^{-1}, a C=N band at about 1670 cm^{-1}, and an N–O band at 974 cm^{-1}. The asymmetric and symmetric C–H stretching vibration of the CH_3 group was observed at 2920-2990 cm^{-1}. Infrared spectra of metal complexes have already been studied intensively, and a metal ion's effects on the vibration frequencies in the ligand have been investigated [17,18]. In the spectra of complex I, the C=N and N–O bands appear at 1655 cm^{-1} and 926 cm^{-1}, respectively. However, in the spectra of complex II, the C=N and N–O bands appear at 1655 cm^{-1} and 968 cm^{-1}. Compared with the infrared spectra of the free ligand, the IR frequency of both C=N and N–O bonds in complexes I and II were shifted to lower frequencies, and it was shown the existence of coordinate bond formation with metals through the nitrogen atoms of the azomethine groups.

3.2. Crystallographic analysis

Crystal structure data for complexes I and II are listed in Table 1. The molecular structures of the two complexes are shown in Figs. 3 and 4. Complex I crystallizes in the triclinic space group Pī, and the structure consists of a discrete complex with the formula $\{Ni(L)_2Cl_2\}$ (I). The Ni^{II} cation occupies an inversion center and is coordinated by two chlorine ligands and two bidentate imidazole oximes through four N atoms. It creates a coordination sphere that possesses a distorted octahedral geometry. The Ni–N(1a), Ni–N(3a), Ni–N(1b), and Ni–N(3b) bond distances are 2.0830(18), 2.0635(18), 2.0836(17), and 2.0546(7) Å, respectively. The Cl(2)–Ni–N(1b), Cl(1)–Ni–N(3b), N(1a)–Ni–N(3a), Cl(1)–Ni–N(3a), and N(1a)–Ni–N(3b) bond angle values of 164.02(5), 98.92(5), 77.81(7), 86.98(5), and 96.20(7)° support the distorted geometry of the molecular structure. The bond distances and angle values are in the normal ranges and are comparable to the corresponding bonds found in similar Nickel oxime Complexes (Table 3a and 3b) [19, 20]. The two imidazole rings are quasiplanar, with a maximum deviation of −0.0783 (23)Å at the C(5a) atom and −0.0271 (23)Å at the C(5b) atom, and form a dihedral angle between them of 87.25(4)°. The crystal packing can be described as alternating double layers along the b-axis (at b = 1/4 and b = 3/4) parallel to the (011) plane (Fig. 2b). The unit cell interacts with each other through the CH…O hydrogen interaction bond between one hydrogen of imidazole cycle and the oxime oxygen atom with distances between 2.29–2.75 Å and angles between 120 and 156°. These interaction bonds

form an infinite, one-dimensional network in one line. Additional intramolecular hydrogen bonds are created through the interaction of the oxime hydrogen atoms with the one-coordinate chlorine. Other bonding parameters are listed in Table 2.

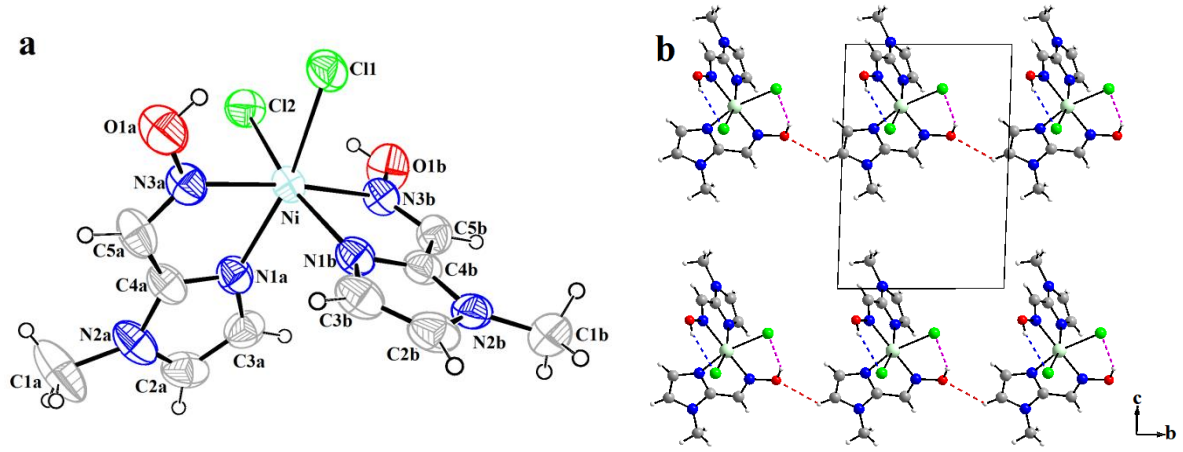

Fig.3. Mercury plots of the molecular structure, hydrogen bonding interactions and crystal packing of I. (a) The molecular structure of I showing the atom numbering scheme. (b) Projection along the b-axis of the atomic arrangement of I showing CH…O intermolecular hydrogen bonds in dashed red lines.

The complex di-μ-chloro-bis[chloro(1-methyl-1H-imidazole-2-carbaldehyde oxime) mercury(II) crystallizes in the monoclinic space group P2/c. The Hg^{II} atom resides on a two-fold axis. The crystal is composed of centrosymmetric dimeric molecules in which a pair of symmetrical chlorine bridges attach two mercury atoms. The coordination geometry around the metal Hg^{II} centre is distorted tetrahedral, with one nitrogen imidazole atom and three chlorine atoms at the corners, with an overall metal-imidazole ligand ratio of 1:1. The Hg–N(1) bond length [2.149(4)Å] compares with the Hg–N bond lengths in reported complexes, for example, 2.270(5) Å in $[HgI_2(bimt)]_2$ {bimt is 2-[(benzimidazolyl)methyl]-1*H*-tetrazole [21] and [2.5226(8) Å in $[[HgBr_2(bmi)_2],]$ [bmi is 1-[(benzotriazol-1-yl)methyl]-1H-1,3-imidazole] [22]. On the other hand, the two chlorine ions are bridged to two metal centers Hg and Hg*i via* a (μ-2–Cl(2), Cl) fashion [Hg–Cl(1) = 2.3359 (16) Å, Hg–Cl(2) = 2.6176 (14)Å] (Table 3b). The bond angles formed by the coordination of the three equatorial donors are 150.18(11)° for N(1)–Hg–Cl(1), 109.14(5)° for Cl(2)–Hg–C(1) and 99.66(10) for Cl(2)–Hg–N(1) (Table 3b). The crystal packing of complex $\{Hg_2(L)_2Cl_4\}$, DMF (II) is directed by hydrogen-bond interactions, with the participation of the imidazole oxime OH-donor centre and DMF Oxygen atoms acting as hydrogen-bond acceptors. The molecules are arranged in two-dimensional square-grid corrugated layers via O–H…O, C–H…O and C–H…Cl hydrogen bonds (Table 2). These layers then stack along a direction, packed as two layers per unit cell (Fig.4b).

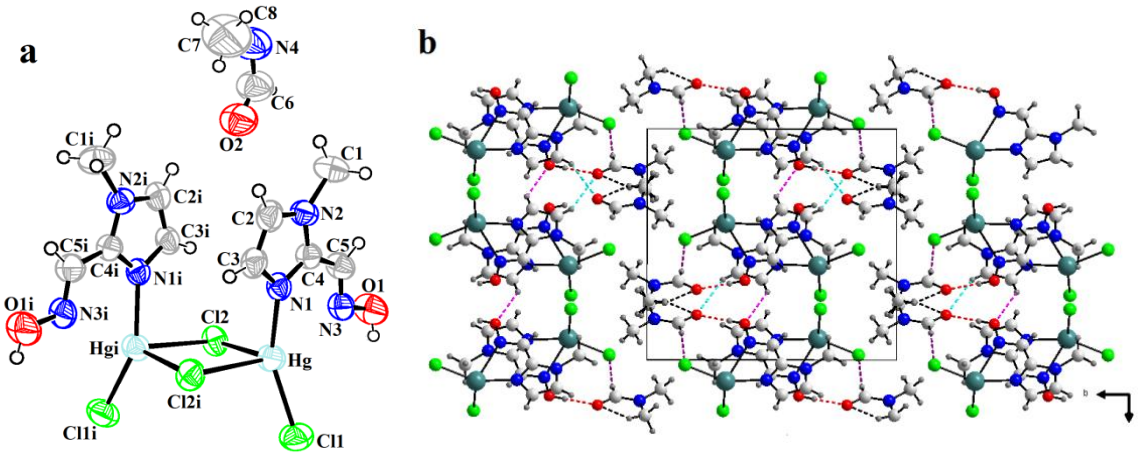

Fig.4. Mercury plots of the molecular structure, hydrogen bonding interactions and crystal packing of II. (a) The molecular structure of II showing the atom numbering scheme. (b) Projection along a axis of the atomic arrangement of II. Dotted lines represent the hydrogen bond.

Table 1

Crystal structure data for complexes (I) and (II).

	$\{Ni(L)_2Cl_2\}$ (I)	**$\{Hg_2(L)_2Cl_4\}$, DMF (II)**
Formula	$C_{10}H_{14}Cl_2N_6NiO_2$	$C_{16}H_{28}Cl_4N_8O_4Hg_2$
Formula weight	379.88	939.44
Crystal habit, color	Prism, green	Prism, Colorless
Crystal system	Triclinic	Monoclinic
Space group	Pī	P 2/c
a (Å)	7.1357(2)	9.0323(5)
b (Å)	8.5591(2)	13.0416(7)
c (Å)	12.7830(3)	14.0145(7)
α (°)	86.948(1)	90
β (°)	78.548 (1)	120.555(3)
γ (°)	84.218(1)	90
Volume (Å^3)	760.85(3)	1421.61(14)
Z, Z'	2, 2	2, 4
Density (calculated, g cm^{-3})	1.658	2.195
Absorption coefficient (mm^{-1})	1.64	11.20
F(000)	388	880
Crystal size (mm)	0.12×0.10×0.08	0.16×0.08×0.05
θ range for data collection (°)	2.4- 27.8	2.3- 26.1
Reflections collected	12093	30724
Independent reflections	3407	4730
R_{int}	0.0242	0.04
Reflections with I ≥ 2σ(*I*)	2653	2999
Number of parameters	194	157
Goodness-of-fit on F^2	1.03	1.05
Final R indices [I ≥ 2σ(*I*)]	0.028	0.0333
R indices [all data]	R_1=0.03, wR_2=0.068	R_1=0.037, wR_2=0.116
Largest difference peak and hole (Å^{-3})	0.29, -0.28	1.46, -0.91
CCDC deposition no.	CCDC 1478614	CCDC 1478614

Table 2

Distances (Å) and angles (°) for Donor-Acceptor in crystals of $\{Ni(L)_2Cl_2\}$ (I) and $\{Hg_2(L)_2Cl_4\}$, DMF (II).

D–H…A	*d*(D–H)	*d*(H…A)	*d*(D–A)	D–H–A	Symmetry
$\{Ni(L)_2Cl_2\}$ (I)					
O(1A)–H(1A)…Cl(1)	0.82	2.35	3.0304(18)	141	xyz
O(1B)–H(1B)… Cl(2)	0.82	2.29	2.989(2)	144	xyz
C(2B)–H(2B)…O(1B)	0.93	2.59	3.162(3)	120	x,1+y,z
C(5A)–H(5A)…O(1A)	0.93	2.55	3.348(3)	144	1-x,2-y,-z
Complex (II)					
O(1)–H(1)…O(2)	0.82	1.85	2.643(10)	164	1-x,1-y,1-z
C(1)–H(1A)…Cl(1)	0.96	2.40	3.253(10)	148	-1/2+x,1-y,-1/2+z
C(1)–H(1B)…O(2)	0.96	2.30	2.945(14)	124	xyz
C(6)–H(6B)…Cl(2)	0.96	2.64	3.5523(12)	160	x,-1+y,z
C(6)–H(6C)…O(2)	0.96	2.42	2.8092(15)	104	xyz

Table 3a

Calculated and experimental geometrical parameters (Å, º) of complex $\{Ni(L)_2Cl_2\}$ (I)

Bond	Exp.(Xray)	Calc. (DFT)	Angles	Exp.(X-ray)	Calc. (DFT)
Ni–Cl(2)	2.4951(6)	2.2292	Cl(2)–Ni–Cl(1)	92.06(2)	104.3614
Ni–Cl(1)	2.4414(6)	2.7601	Cl(2)–Ni–N(3a)	96.10(5)	91.9362
Ni–N(1a)	2.0830 (18)	3.0664	Cl(2)–N –N(3b)	86.19(5)	90.9149
Ni–N(1b)	2.0836 (17)	1.9462	Cl(2)–Ni–N(1b)	164.02(5)	168.9215
Ni–N(3a)	2.0635 (18)	1.9072	Cl(1)–Ni–N(3a)	86.98(5)	89.0335
Ni–N(3b)	2.0546 (17)	1.927	Cl(1)–N –N(3b)	98.92(5)	91.3739
C(4a)–N(1a)	1.325(3)	1.3293	Cl(1)–Ni–N(1b)	90.30(5)	84.3893
C(5a)–N(3a)	1.279(3)	1.2894	N(1a)–Ni–N(3a)	77.81(7)	68.7417
C(5b) –N((3b)	1.268(3)	1.2927	N(1a)–Ni–N(3b)	96.20(7)	110.2224
O(1b)–N(3b)	1.376(2)	1.3467	N(1a)–Ni–N(1b)	90.41(7)	86.4677

Table 3b

Calculated and experimental geometrical parameters (Å, º) of complex $\{Hg_2(L)_2Cl_4\}$, DMF (II)

Bond	Exp. (X–ray)	Calc. (DFT)	Angles	Exp. (X–ray)	Calc. (DFT)
Hg–Cl(1)	2.3359(16)	2.4600	Cl(2)–Hg–Cl(1)	109.14(5)	126.008
Hg–Cl(2)	2.6176(14)	2.6236	Cl(2)–Hg– N(1)	99.66(10)	94.6324
Hg–N(1)	2.149(4)	2.4516	Hg–Cl(2)–Hgi	87.93(4)	89.8719
C(4)–N(1)	1.323(6)	1.3326	Hg–N(1)–C(3)	129.4(3)	131.6633
C(4)–N(2)	1.340(6)	1.365	C(5)–C(4)–N(1)	125.4(4)	124.0963
C(5)–N(3)	1.250(7)	1.2806	N(1)–C(4)–N(2)	109.2(4)	110.2267
N(1)–C(3)	1.369(6)	1.368	C(4)–C(5)–N(3)	118.8(4)	114.6725
N(3)–O(1)	1.377(5)	1.355	C(4)–N(1)–C(3)	107.3(4)	107.0889
N(2)–C(2)	1.362(7)	1.3828	C(5)–N(3)–O(1)	111.6(4)	117.1302
C(2)–C(3)	1.354(7)	1.3728	N(1)–C(3)–C(2)	108.6(4)	109.1669

3.3. Hirshfeld surface analysis

The program Crystal Explorer 3.1 [23] was used to generate the Hirshfeld surface analysis [24], which has been undertaken better to understand the intermolecular interactions in the crystal structure. The d_{norm} (normalized contact distance) representation mode was used; red spots on the surface indicate the presence of atoms in very close proximity to the outside of the Hirshfeld surface, and the white surface means that the atoms are in medium proximity. The blue surface shows little proximity of outside atoms. The Hirshfeld surface (Fig. 5 and 7) shows red spots corresponding to H…Cl/Cl…H and H…O/O…H close contacts, which are due to the O–H…Cl, C-H…O and O-H…O hydrogen bonds for both compounds.

The corresponding two-dimensional fingerprint plots [25] were used for decoding and quantifying the intermolecular interactions in the crystal lattice are shown in Figures 6 and 8. The relative contributions of the various intermolecular contacts are illustrated in Fig. 6b and Fig. 8b. In the complex $\{Ni(L)_2Cl_2\}$ (I), the H…H contacts dominate. Its relative contribution to the total surface is 41%. The H…Cl/Cl…H contacts also contribute significantly to the total surface with 26%. Furthermore, the O…H/H…O contacts display a notable proportion of 12%. In complex $\{Hg_2(L)_2Cl_4\}$, DMF (II), the H…H and H…Cl/Cl…H contacts dominate; their relative contributions to the total surface are 35% and 36%, respectively. The H…O/O…H contacts also contribute significantly to the total surface with 13%.

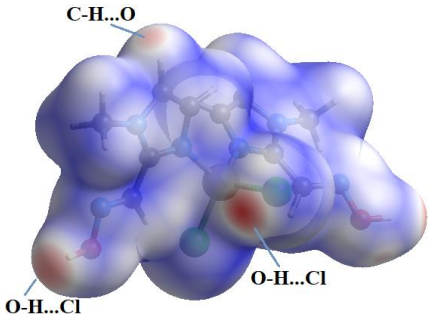

Fig.5. View of the 3D Hirshfeld surface mapped over d_{norm} of complex $\{Ni(L)_2Cl_2\}$ (I).

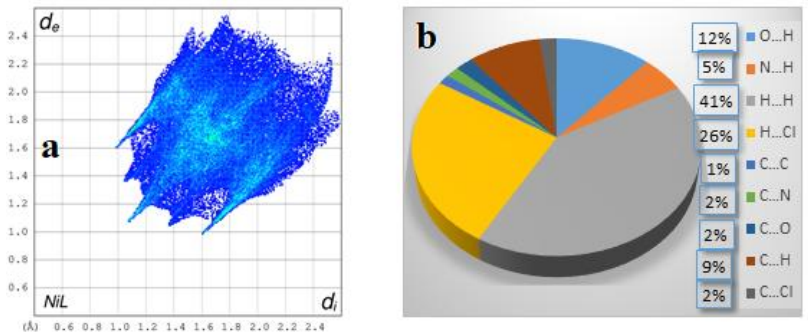

Fig. 6. (a) The 2D fingerprint plot. (b) Relative contributions to the Hirshfeld surface area for the various close intermolecular contacts in complex $\{Ni(L)_2Cl_2\}$ (I).

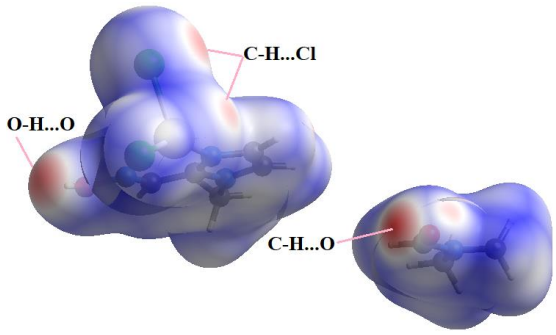

Fig. 7. View of the 3D Hirshfeld surface mapped over d_{norm} of complex $\{Hg_2(L)_2Cl_4\}$, DMF (II).

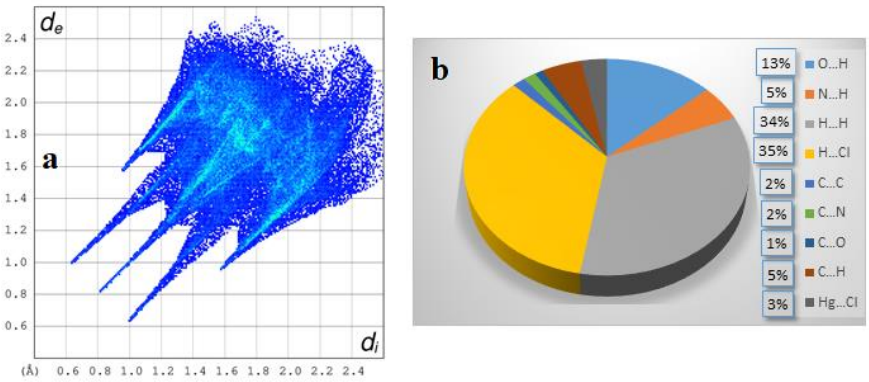

Fig. 8. (a) The 2D fingerprint plot. (b) Relative contributions to the Hirshfeld surface area for the various close intermolecular contacts in complex $\{Hg_2(L)_2Cl_4\}$, DMF (II).

3.4. Electrochemical study

The CV measurements were employed to investigate the redox behaviour of the compounds and to estimate the highest occupied molecular orbital (HOMO) and lowest unoccupied molecular orbital (LUMO) energy levels of L from the onset of the oxidation and onset of the reduction potentials [26]. CV of L and its complexes were recorded at 10^{-3} M in a deoxygenated dimethylsulfoxide (DMSO) solution mixed with 0.1 M of Bu_4NBF_4 as supporting electrolyte, with a scan rate of 100 mV/s. L, complex $\{Ni(L)_2Cl_2\}$ and complex $\{Hg_2(L)_2Cl_4\}$ were investigated voltammetrically within the potential window from -1.2 V to +1.2 V, from -0.75 V to +1.5 V and from -2 V to +2 V, respectively.

Table 4

Electrochemical HOMO, LUMO and band-gap values of Ligand.

	E^{ox}_{onset}(V)[a]	E^{red}_{onset}(V)[b]	E_{HOMO}(eV)[c]	E_{LUMO}(eV)[d]	E_g^{el}(eV)[e]
Ligand	0.78	-0.73	-5.18	-3.67	1.51

a *The onset potential of oxidation .* ***b*** *The onset potential of reduction.* ***c*** E_{HOMO} *(eV) = - [*E^{ox}_{onset} *(vs. SCE) + 4.4].* ***d*** E_{LUMO} *(eV) = - [*E^{red}_{onset} *(vs. SCE) + 4.4].* ***e*** *Energy of the band-gap calculated from the difference between the energy of the HOMO and the LUMO band.*

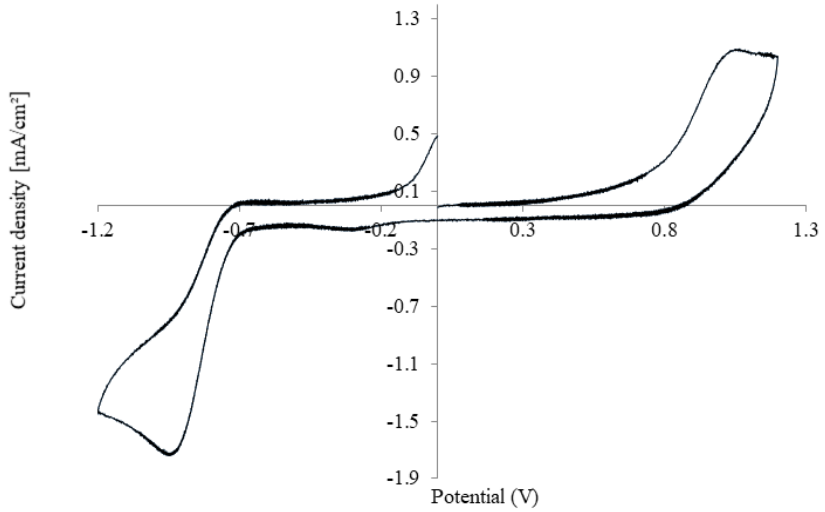

Fig.9. Cyclic voltammogramm recorded with 5.0×10^{-3} M of Ligand in Bu_4NBF_4 (0.1M)/DMSO solution at a scan rate of 100 mV/s.

The cyclic voltammogram of L displayed one irreversible anodic peak at 1.06 V and one irreversible cathodic peak at - 0.94 V. The anodic peak was assigned to the oxidation of the oxime group, while the cathodic peak was assigned to its reduction (Fig. 9) [27]. The cyclic voltammetry of complex $\{Ni(L)_2Cl_2\}$ showed a decrease in the current intensity of the anodic peak assigned to the oxidation of the oxime group, which confirms its participation in the coordination. In addition, a new redox couple appears with a reduction peak recorded at -0.18V and an associated oxidation peak recorded at 0.563V (Fig. 10). This redox peak was assigned to the Ni^{+2}/Ni^0 redox couple [28]. We also note the disappearance of the reduction peak of the oxime group, which is probably due to the participation of its nitrogen atom in the coordination.

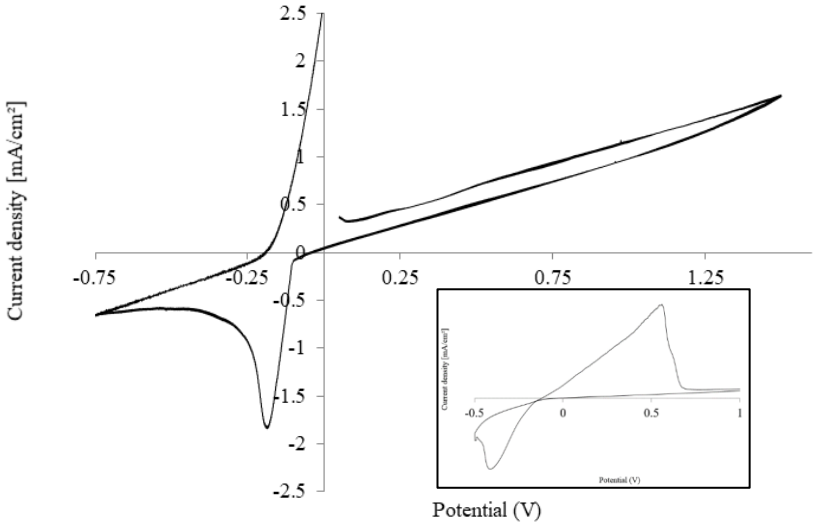

Fig.10. Cyclic voltammogramm recorded with 5.0×10^{-3}M of complex $\{Ni(L)_2Cl_2\}$ in Bu_4NBF_4 (0.1M)/DMSO solution at a scan rate of 100 mV/s.

The voltammogram of complex $\{Hg_2(L)_2Cl_4\}$ shows two redox systems. The cathodic peaks are recorded at -0.86 and -0.53 V, while the corresponding anodic peaks at 0.08 and 0.5 V (Fig. 11), respectively. These systems are associated to the electrochemical response of the couples Hg^{+2} / Hg^{+1} and Hg^{+1} / Hg^{0} [29]. Moreover, the oxidation peak of the oxime group is still present, but has lost its intensity (Fig. 11). This behavior confirms that the oxime group do not participate in the complex $\{Hg_2(L)_2Cl_4\}$ coordination, unlike complex $\{Ni(L)_2Cl_2\}$. The presence of the reduction peak of the oxime cannot be confirmed because it overlaps with that of the metal ion.

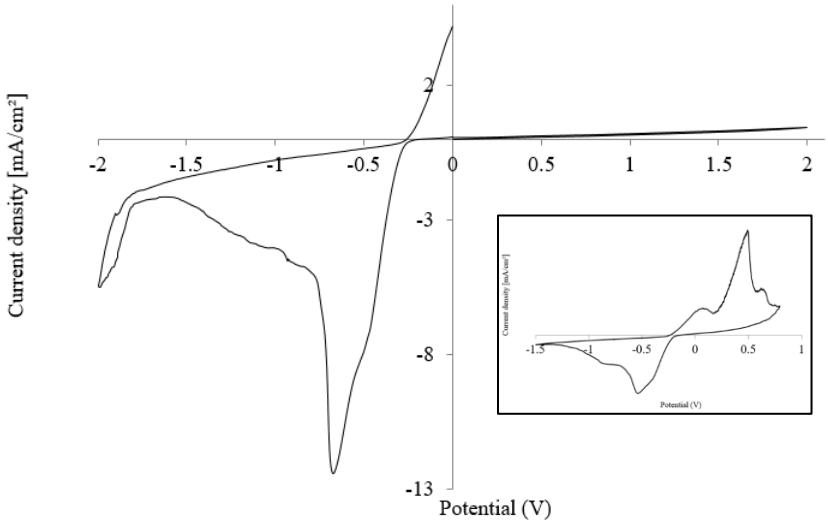

Fig.11. Cyclic voltammogramm recorded with 5.0×10^{-3}M of complex $\{Hg_2(L)_2Cl_4\}$ in Bu_4NBF_4 (0.1M)/DMSO solution at a scan rate of 100 mV/s.

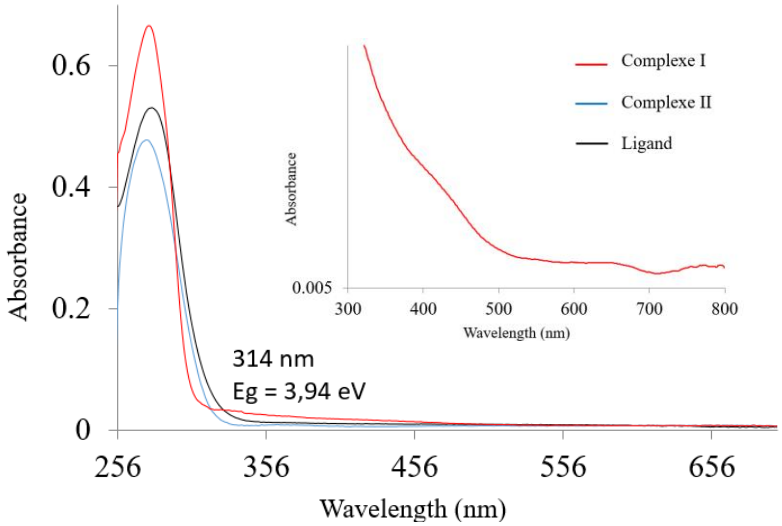

Fig.12. UV-vis absorption spectra of L (black), complex $\{Ni(L)_2Cl_2\}$ (I) (red) and complex$\{Hg_2(L)_2Cl_4\}$ (blue).

Figure 12 depicts the UV-vis spectra of L and its complexes in the DMSO. The absorption maximum (λ_{max}) of L, centered at 281 nm, is due to a π-π^* transition of the imidazole ring [30]. This absorption shifts to 278 nm for the two complexes, probably because of the ligand

energy change after coordination with the metal or for the overlap of a π-π* transition by a charge transfer band resulting from coordination [31]. Indeed, in transition metal complexes, the electron distribution exchanges between the metal and the ligand lead to some intense absorption bands called charge transfer (CT) [32] that can appear in the ultraviolet and/or visible portions of the spectrum [31]. Moreover, a hyperchromic effect was observed for this band of complex $\{Ni(L)_2Cl_2\}$. This effect should be related to a metal-ligand charge transfer (MLCT) from Ni^{II} to C=N–O (ligand) [33]. In the imidazole unit present in the octahedral d^6 Ni-complex which is generally considered to be a moderate s-donor ligand [34,35], electrons can be excited not only from *t2g* to *eg*, but also from the ligands *s* orbitals to *eg* [31]. The $s \rightarrow eg$ excitation results in a charge transfer transition from the ligand to metal (LMCT) recorded at 427 nm, while the $t2g \rightarrow eg$ leads to a weak band d-d transition recorded at 641 nm. For complex $\{Hg_2(L)_2Cl_4\}$, no d–d transitions were observed in the spectrum as expected for the d^{10} Hg^{II} complex.

3.5. Theoretical study

The ligand, complex $\{Ni(L)_2Cl_2\}$ and complex $Hg_2(L)_2Cl_4\}$ without DMF molecule were modelled using ACD Chemsketch software [36] and optimized at the DFT/B3LYP/(6-31G + (d) for C, H, O, N, Cl atoms and the Stuttgart/Dresden effective core potentials basis set (SDD) for Ni and Hg atoms) level in the gas phase. The Stuttgart-Dresden effective core potential ECPs (SDD) were used for metal atoms. The same level of theory was used for vibrational frequency calculations to confirm that the optimized geometries were reel minima. No imaginary frequencies were observed for the three compounds. All DFT calculations were conducted via Gaussian 09W software [37]. Visualization and result analysis were performed with the GaussView 5 program [38].

A comparative analysis of the essential bond lengths and angles was realized for both complexes (Tables 3a, 3b). It shows a good harmony between calculated and experimental data globally. Frontier orbitals, LUMO and HOMO, are very helpful for the molecular reactivity and stability prediction of one given compound. These orbitals were plotted, and their energies were calculated for the three studied molecules (Figure 13). Frontier orbital analysis showed that they are homogeneously deployed for the ligand. However, HOMO of the complex $\{Ni(L)_2Cl_2\}$ was localized on the chlorine and nickel atoms, while LUMO was located on one half of its structure. For the complex $\{Hg_2(L)_2Cl_4\}$, both HOMO and LUMO were mainly situated on the imidazole oxime ligand.

The value of the gap (the energy difference between the frontier orbitals) for the ligand and its two complexes is comparable, showing similar stability. However, the smallest value corresponds to complex {$Ni(L)_2Cl_2$}, thus reflecting a slightly higher reactivity for the latter. Frontier orbitals' energies are used to calculate the global reactivity descriptors for the studied compounds (Table 6). Time-dependent density functional theory (TD-DFT) computation was also carried out at the same level of the theory in DMSO using the IEF-PCM salvation model, to predict the UV-Vis electronic absorption spectra of our complexes. The major transition and the oscillator strength (*f*), as well as the energy of the main bonds, were also explored (Table 5).

Table 5

Major transition, energy and oscillator strength (*f*) of the main bonds of the three compounds' UV-Vis spectra, calculated in DMSO (IEF-PCM) at the DFT/B3LYP/(6-31G + (d) for C, H, O, N, Cl atoms and SDD for Ni and Hg atoms) level.

	$\lambda_{exp.}$(nm)	$\lambda_{theo.}$ (nm)	E(eV)	*f*	Main transition	Contribution
Ligand	281	271.51	4.5664	0.5118	HOMO → LUMO	98.25
Complex {$Ni(L)_2Cl_2$}	279	293.20	4.2287	0.3265	HOMO → LUMO+3	39.49%
Complex {$Hg_2(L)_2Cl_4$}	278	287.78	4.3083	0.2099	HOMO → LUMO+2	64.77%

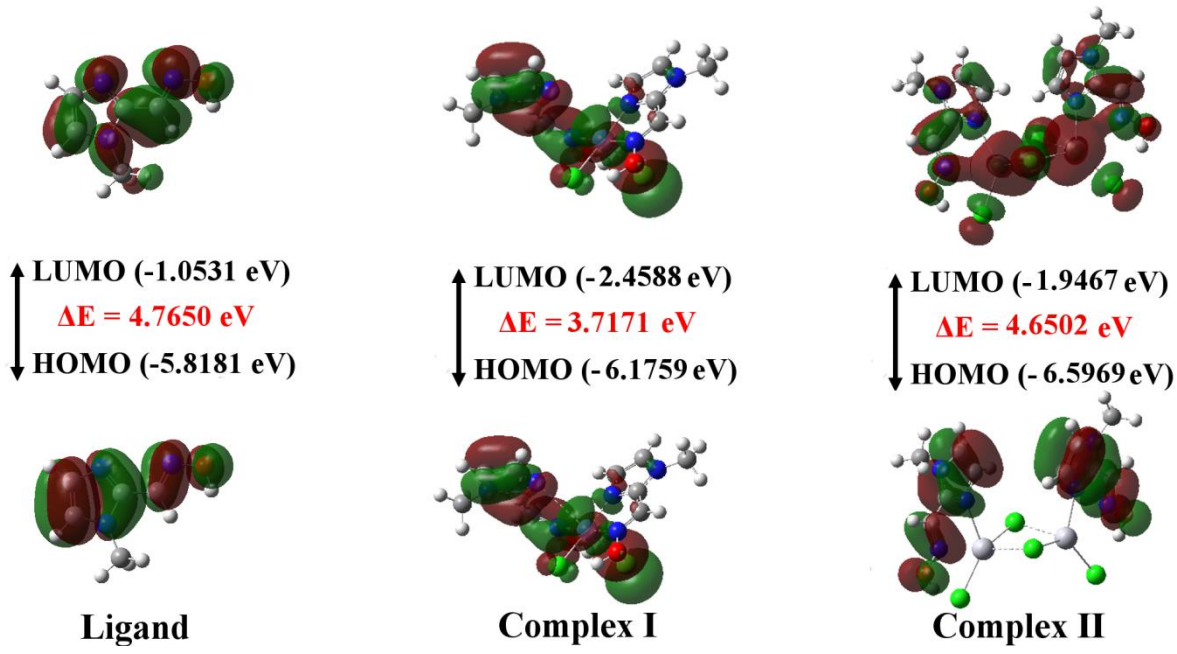

Fig.13. Frontier orbitals' contour surfaces and energies for the ligand, complex {$Ni(L)_2Cl_2$} and complex {$Hg_2(L)_2Cl_4$}.

Table 6

Global reactivity descriptors calculated in vacuum (DFT/B3LYP/Genecp) for the ligand, complex $\{Ni(L)_2Cl_2\}$ (I) and complex $\{Hg_2(L)_2Cl_4\}$ **(**I)I.

Parameters (eV)	**Ligand**	**Complex $\{Ni(L)_2Cl_2\}$**	**Complex $\{Hg_2(L)_2Cl_4\}$**
E_{HOMO}	-5.8181	-6.1759	-6.5969
E_{LUMO}	-1.0531	-2.4588	-1.9467
Energy band gap $\lvert E_{LUMO} - E_{HOMO}\rvert$	4.7650	3.7171	4.6502
Ionization potential ($I = - E_{HOMO}$)	5.8181	6.1759	6.5969
Electron affinity ($A = - E_{LUMO}$)	1.0531	2.4588	1.9467
Chemical hardness ($\eta = (I-A)/2$)	2.3825	1.8585	2.3251
Chemical softness ($\zeta = ½\ \eta$)	1.1912	0.2690	0.2150
Electronegativity ($\chi = (I+A)/2$)	3.4356	4.3174	4.2718
Chemical potential ($\mu = - \chi$)	-3.4356	-4.3174	-4.2718
Electrophilicity ($\omega = \mu^2/2\eta$)	2.4771	5.0146	3.9242
Maximum charge transfer index ($\Delta N_{max.} = -\mu/\eta$)	1.4420	2.3230	1.8373

4. Conclusion

In summary, we have synthesized two new mononuclear compounds from 1-methyl-1*H*-imidazole-2-carbaldehyde oxime ligand with MII cations, namely $\{Ni(L)_2(Cl)_2\}$, (I) and $\{Hg_2(L)_2Cl_4\}$, DMF (II). Spectroscopic methods characterized both complexes and their structures were confirmed by X–ray crystal structure analysis. The *d*8 configuration of the NiII cation and the *d*10 configuration of the HgII allow the self-assembly of MII with the organic ligand in a distorted octahedral geometry for complex (I) and distorted tetrahedral geometry for complex (II). Hydrogen-bonding interactions help to consolidate both crystal structures. The Hirshfeld surface shows the domination of H…Cl/Cl…H and H…O/O…H contacts which are due to the O–H…Cl, C-H…O and O-H…O hydrogen bonds for both compounds. Cyclic voltammetry was used to investigate the chemical reactivity of the studied compounds, confirming the participation of the oxime group in the coordination in the case of the complex $\{Ni(L)_2Cl_2\}$. DFT calculations exhibited comparable experimental and theoretical findings. Exploration of the natural spectral electronic transitions showed a HOMO → LUMO transition for the ligand, while other orbitals are involved for complex $\{Ni(L)_2Cl_2\}$and complex$\{Hg_2(L)_2Cl_4\}$.

Declaration of Competing Interest

The authors declare that they have no known competing financial interests or personal relationships that could have appeared to influence the work reported in this paper.

CRediT authorship contribution statement

Mahdi Bouchouit: Investigation, Writing –original draft. **Hadjer Belahlou:** Investigation. **Sofiane Bouacida:** Supervision and data collection. **Mounia Guergouri:** Electrochemical analysis. **Rafik Bensegueni:** Theoretical Analysis. **El-Eulmi Bendeif:** XRD analyses, review & editing. **Karim Bouchouit**: Supervision and data collection**. Abdelmalek Bouraiou:** Supervision, Methodology, Writing, review & editing.

Acknowledgements: We thank the Ministère de l'Enseignement Supérieur et de la Recherche Scientifique – Algérie (MESRS) for financial support. We thank the HPC Center of Constantine 1 University for providing the computing infrastructure used in our calculations.

References

[1] W. Kaim, B. Schwederski, *Bioinorganic Chemistry: Inorganic Elements in the chemistry of Life, an introduction and guide, Inorganic Chemistry: A Textbook series*, John Wiley & Sons, Chichester, 1994.

[2] J. C. Bailar, Jr. and D. H. Busch, in J. C. Bailer, Jr. (Ed.), *The Chemistry of the Coordination Compounds*, Reinhold, New York, 1956.

[3] R. C. Mehrotra, A. K. Rai, A. Singh, R. Bohra, 1975. Inorg. Chim. Acta 13 (1975) 91-103. https://doi.org/10.1016/S0020-1693(00)90182-8.

[4] M. H. Chao, S. Kumaresan, Y. S. Wen, S. C. Lin, J. R. Hwu, K. L. Lu, Organometallics, 19 (2000) 714-717. https://doi.org/10.1021/om990441v.

[5] C. J. Milios, T. C. Stamatatos, S. P. Perlepes, Polyhedron 25 (2006) 134-194. https://doi.org/ 10.1016/j.poly.2005.07.022.

[6] A. Kilic, M. Durgun, N. Yorulmaz, R. Yavuz, J. Mol. Struct. 1174 (2018) 25-31. https://doi.org/10.1016/j.molstruc.2018.03.121.

[7] V. Kamat, K. Kumara, K. Naik, A. Kotian, P. Netalkar, N. Shivalingegowda, N. K. Lokanath, V. Revankar, J. Mol. Struct. 1149 (2017) 357-366. https://doi.org/10.1016/j.molstruc.2017.07.109.

[8] Ş. Karadeniz, C.Y. Ataol, O. Şahin, Ö. İdil, Hü. Bati, J. Mol. Struct. 1161 (2018) 477-485. https://doi.org/ 10.1016/j.molstruc.2018.01.087.

[9] A. Ofori, S. Suvanto, S. Jääskeläinen, L. Koskinen, I. O. Koshevoy, P. Hirva, *Cryst. Growth Des.* 2016, 16, 1, 255–264. https://doi.org/10.1021/acs.cgd.5b01222.

[10] M. C. Burla, R. Caliandro, M. Camalli, B. Carrozzini, G. L. Cascarano, L. De Caro, C. Giacovazzo, G. Polidori, R. Spagna, J. Appl. Cryst. 38 (2005) 381-388. https://doi.org/10.1107/S002188980403225X.

[11] G. M. Sheldrick, *Acta Cryst. A* 64 (2008) 112-122. https://doi.org/ 10.1107/S0108767307043930.

[12] L. J. Farrugia, *J. Appl. Cryst.* 45 (2012) 849-854. https://doi.org/ 10.1107/S0021889812029111.

[13] G. M. Sheldrick, SADABS (Bruker AXS Inc.: Madison, Wisconsin, USA), 2002.

[14] D. C. Bebout, M. M. Garland, G. S. Murphy, E. V. Bowers, C. J. Abelt, R. J. Butcher, Dalton Trans. 12 (2003) 2578-2584. https://doi.org/10.1039/B300001J.

[15] C. M. Fierro, P. D. Smith, P. N. Horton, M. B. Hursthouse, M. E. Light, Inorganica Chim. Acta, 368 (2011) 257–262. https://doi.org/ 10.1016/j.ica.2010.12.051.

[16] M. E. Keeney, K. Osseo-Asare, Polyhedron, 3 (1984) 64-649. https://doi.org/10.1016/S0277-5387(00)88001-8.

[17] A. S. El-Tabla, M. M. Abd El-Waheedb, M. M. E. Shakdofac, N. A. Abou El-Fadla, Main Group Chem. 12 (2013) 153–168. https://doi.org/10.3233/MGC-130099.

[18] J. J. Norman, Can. J. Chem. 40 (1962) 2023-2029. https://doi.org/10.1139/v62-310.

[19] S. Mukherjee, B. A. Patel, S. Bhaduri, Organometallics, 28 (2009) 3074–3078. https://doi.org/10.1021/om900080h.

[20] V. Yu. Kukushkin, A. J. L. Pombeiro, Coord. Chem. Rev. 181 (1999) 147–175. https://doi.org/10.1016/S0010-8545(98)00215-X.

[21] Y. N. Ding, X. L. Zhou, G. H. Jin, D. Zhao, X. R. Meng, Synth. React. Inorg. Met.-Org. Nano-Met. Chem. 42 (2012) 438-443. https://doi.org/10.1080/15533174.2011.611848.

[22] X. Wei, J.-H. Li, Q.-Y. Huang, X.-R. Meng, Acta Crystallogr. C Struct. Chem. 73 (2017) 314-318. https://doi.org/10.1107/s2053229617003199.

[23] S. K. Wolff, D. J. Grimwood, J. J. McKinnon, M. J. Turner, D. Jayatilaka, M. A. Spackman, Crystal Explorer 3.1, University of Western Australia, 2013.

[24] C. Jelsch, K. Ejsmont, L. Huder, IUCr J. 1 (2014) 119-128. https://doi.org/10.1107/ S2052252514003327.

[25] J. J. McKinnon, D. Jayatilaka, M. A. Spackman, *Chem. Commun*. 37 (2007) 3814-3816. https://doi.org/10.1039/b704980c.

[26] A. P. Kulkarni, C. J. Tonzola, A. Babel, S. A. Jenekhe, *Chem. Mater*. 16 (2004) 4556–4573. https://doi.org/10.1021/cm049473l.

[27] B. Soucaze-Guillous, H. lund. Acta. Chemica Scandinavica, 52 (1998) 417- 424. https://doi.org/10.3891/acta.chem.scand.52-0417.

[28] V. Ramirez-Delgado, G. Osorio-Monreal, L. F. Hernandez-Ayla, Y. Reyes-Vidal, J. C. Garcia-Ramos, L. Ruiz-Azuara, L. Ortiz-Frade. *J. Mex. Chem. Soc*. 59 (2015) 294-301.

[29] A. Safavi, M. B. Gholivand, *Can. J. Chem*. 74 (1996) 95-102. https://doi.org/10.1139/v96-012.

[30] S. K. Jawad, E. k. kareem, I. R. Ali. Baghdad Sci. J. 10(2) (2013) 420-431, https://doi.org/10.21123/bsj.10.2.420-431.

[31] G. L. Miessler, *Inorganic chemistry*. — Fifth edition / G. L. Miessler, St. Olaf College, P. J. Fischer, Macalester College, 2014.

[32] C. E. Housecroft, A. G. Sharpe. "Outer Sphere Mechanism." *Inorganic Chemistry*. Harlow, England: Pearson Prentice Hall, 2008.

[33] J. M. dos Reisa, B. F. R. Martinsa, L. R. V. Favarina, P. P. Rosaa, G. B. Laranjeiraa,C. F. Almeida, S. C. de Oliveiraa, L. Pizzutib, A. M. Júniora, G. A. Casagrandea. *Orbital: Electron. J. Chem*. 9(1) (2017) 89-94, https://doi.org/10.17807/orbital.v9i1.952.

[34] R. J. Sundberg and R. B. Martin, Chem. Rev. 74, (1974) 471–517. https://doi.org/10.1021/cr60290a003.

[35] M. A. Trojer, Alireza Movahedi, Hans Blanck, and Magnus Nydén. J. Chem. *(*2013), 946739, https://doi.org/10.1155/2013/946739.

[36] ACD/ChemSketch, version 12.01, Advanced Chemistry Development, Inc., Toronto, ON, Canada, www.acdlabs.com, 2009.

[37] Gaussian 09, Revision E.02, M. J. Frisch, G. W. Trucks, H. B. Schlegel, G. E. Scuseria, M. A. Robb, J. R. Cheeseman, G. Scalmani, V. Barone, G. A. Petersson, H. Nakatsuji, X. Li, M. Caricato, A. Marenich, J. Bloino, B. G. Janesko, R. Gomperts, B. Mennucci, H. P. Hratchian, J. V. Ortiz, A. F. Izmaylov, J. L. Sonnenberg, D. Williams-Young, F. Ding, F. Lipparini, F. Egidi, J. Goings, B. Peng, A. Petrone, T. Henderson, D. Ranasinghe, V. G. Zakrzewski, J. Gao, N. Rega, G. Zheng, W. Liang, M. Hada, M. Ehara, K. Toyota, R. Fukuda, J. Hasegawa, M. Ishida, T. Nakajima, Y. Honda, O. Kitao, H. Nakai, T. Vreven, K. Throssell, J. A. Montgomery, Jr., J. E. Peralta, F. Ogliaro, M. Bearpark, J. J. Heyd, E. Brothers, K. N. Kudin, V. N. Staroverov, T. Keith, R. Kobayashi, J. Normand, K. Raghavachari, A. Rendell, J. C. Burant, S. S. Iyengar, J. Tomasi, M. Cossi, J. M. Millam, M. Klene, C. Adamo, R. Cammi, J. W. Ochterski, R. L. Martin, K. Morokuma, O. Farkas, J. B. Foresman, and D. J. Fox, Gaussian, Inc., Wallingford CT, 2016.

[38] R. Dennington, T. A. Keith, J. M. Millam, GaussView, Version 5.0.9. Shawnee Mission, KS: Semichem; 2016.